Probing Strain-Tunable Guided Modes in Graphene Waveguide by Photon-Assisted Tunneling

2013 Appl. Phys. Express 6 065102

(http://iopscience.iop.org/1882-0786/6/6/065102)

Applied Physics Express **6** (2013) 065102
http://dx.doi.org/**10.7567/APEX.6.065102**

Probing Strain-Tunable Guided Modes in Graphene Waveguide by Photon-Assisted Tunneling

Yunhua Wang[1], Yulan Liu[2]*, and Biao Wang[1]*

[1] *School of Physics and Engineering, Sun Yat-sen University, Guangzhou 510275, China*
[2] *School of Engineering, Sun Yat-sen University, Guangzhou 510275, China*
E-mail: stslyl@mail.sysu.edu.cn; wangbiao@mail.sysu.edu.cn

Received April 18, 2013; accepted May 10, 2013; published online May 28, 2013

Strain effect on guided modes and electron transmission through the strained graphene waveguide with oscillating potential are explored theoretically. It is found that the guided mode in the waveguide can be controlled by zigzag or armchair direction strain. The transmission spectrum obtained displays a sharply asymmetric tunneling peak, where the energy difference between the tunneling peak and guided mode is equal to the photon induced by the oscillating potential. In view of the quantitative relationship, we propose the photon-assisted tunneling to probe the strain-tunable guided modes.

Owing to the similarity between the linear dispersion for electrons in graphene and energy-momentum relationship for light, the analogous light phenomenon of electrons in graphene has attracted considerable attention in quantum transport and application of carbon-based nanoelectronics.[1–12] As one of these significant applications, the graphene waveguide has been theoretically proposed on the basis of magnetic field,[5] combination of magnetic and electric fields,[6,7] geometric constraints,[8] or quantum well induced by an electrostatic potential,[9–12] due to their confinement effects for electrons in graphene, respectively. By analogy of guiding light in a fiber, the bound state serves as a guided mode and guides electrons in a graphene waveguide. With the rapid development of electron-beam lithography technology, P (hole-like) or N (electron-like) regions in graphene have been achieved by using a combination of top/bottom gates.[13] Recently, the graphene waveguide based on the gate-controlled quantum well has been fabricated and its guided efficiency has also been measured experimentally by the four-terminal electrode method.[12]

Usually, the coupling between a substrate and graphene can lead to strain for the graphene placed on the substrate. In addition, a suitable substrate patterning can induce a distribution of local strain profiles, which may provide an important path for achieving multiple nanodevices in the same graphene sheet.[14] Some investigations also show that reversible and controlled strain in graphene can be realized by using a uniform planar tension[15] or atomic force microscope (AFM) tip.[16] Owing to the large elastic deformation of up to 20% for graphene,[17] the strain in graphene has the advantage of high tunability. Moreover, the strain and some strain-induced change in graphene electronic and optical properties can be quantitatively measured by Raman spectroscopy.[18,19] On the other hand, it is demonstrated that strain has a strong influence on the electric structure in graphene-based nanostructures, such as a band gap opening only along the zigzag direction strain with a magnitude larger than 23%,[15] Dirac cone's deformation resulting in anisotropic group velocity,[20,21] and K (K′) point displacement introducing a pseudomagnetic field.[21,22] As a result, the strain-induced anisotropic velocity and pseudomagnetic field can be used to manipulate the electronic transport in these nanostructures. One of our aims in this letter is to report the strain effect on electronic transport of a graphene waveguide, including the guided modes and tunneling through the quantum well.

As previously mentioned, a graphene waveguide has been proposed theoretically and prepared experimentally. However, up to now, the guided mode as the main characteristic of the graphene waveguide has not been detected, due to the lack of an available probing method. In this letter, we will present an available approach to examine the guided mode and the strain effect on the guided mode, based on the photon-assisted tunneling.[23] We consider the strained waveguide in the presence of an oscillating potential supplying the photons, which are absorbed or emitted by incident electrons so as to tunnel through the confined region of the waveguide by virtue of the bound states. The transmission spectrum exhibits a strongly asymmetric tunneling peak, which manifests the existence of the guided mode.

Hamiltonian and wave functions. We consider a graphene quantum well, where uniaxial strain is applied inside the well region with time-periodic oscillating potential realized by a top or bottom gate. Low-energy electrons near the K point can be described by the effective Hamiltonian

$$H = \begin{cases} \hbar v_{\rm f}[\boldsymbol{\sigma}_x p_x + \boldsymbol{\sigma}_y p_y] & (|x| > w/2) \\ H_{\rm s} - U_0 + U_1 \cos\omega t & (|x| \le w/2) \end{cases}, \tag{1}$$

where $\boldsymbol{\sigma}_x$ and $\boldsymbol{\sigma}_y$ are Pauli spin matrices, U_0 is the depth of the potential well, and U_1 and ω are the magnitude and frequency of the ac potential, respectively. In Eq. (1), the strain-dependent Hamiltonian $H_{\rm s}$ reads[21]

$$H_{\rm s} = \hbar v_{\rm f} U^{\dagger}(\theta)[\boldsymbol{\sigma}_x(1-\lambda_x\varepsilon)q_x + \boldsymbol{\sigma}_y(1-\lambda_y\varepsilon)q_y]U(\theta), \tag{2}$$

where θ is the angle between the strain direction and graphene zigzag direction (labeled by x-direction), $\lambda_x = 2.2$, $\lambda_y = -0.308$, $U(\theta) = \mathrm{diag}(1, e^{-i\theta})$ is the unitary matrix, ε is the magnitude of strain, and $\boldsymbol{q} = (q_x, q_y)^{\rm T}$ measures the wave vector displacement from the shifted Dirac points $q_{\rm D} = \pm[\kappa_0\varepsilon(1+\mu)\cos 3\theta/a_0, -\kappa_0\varepsilon(1+\mu)\sin 3\theta/a_0]^{\rm T}$,[21] where $\kappa_0 \approx 1.6$ and $a_0 = 0.142$ nm is the C–C distance. Note that the energy gap is not considered because the magnitude of strain in this work is limited within 23%, where the gap cannot be opened up.[15] Taking into account the Floquet theorem and the conservation of k_y, one can write the wavefunctions as

$$\boldsymbol{\psi}(x,y,t) = \begin{bmatrix} \psi_{\rm A}(x,t) \\ \psi_{\rm B}(x,t) \end{bmatrix} \exp(ik_y y)\exp\left(-i\frac{E_{\rm F}t}{\hbar}\right), \tag{3}$$

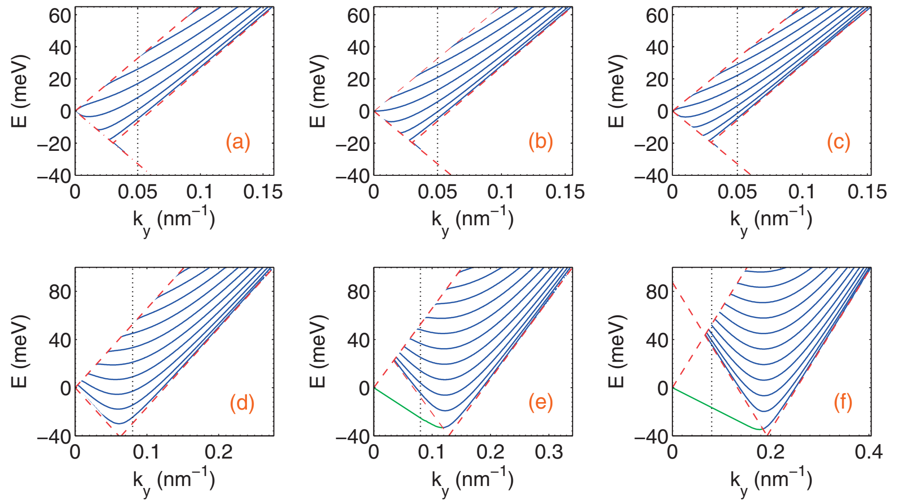

Fig. 1. Energy spectrum $E(k_y)$ for $U_0 = 40$ meV, $U_1 = 0$ meV, and $w = 150$ nm; under zigzag direction strain: (a) $\varepsilon = 2\%$, (b) $\varepsilon = 8\%$, and (c) $\varepsilon = 14\%$; under armchair direction strain: (d) $\varepsilon = 0.5\%$, (e) $\varepsilon = 1\%$, and (f) $\varepsilon = 1.5\%$.

where $E_F = E + n\hbar\omega$ (n is an integer) is the Floquet energy eigenvalue and $\Psi_{A(B)}(x,t) = \Psi_{A(B)}(x, t+T)$ is time-periodic functions with period $T = 2\pi/\omega$. Substituting Eq. (3) into Eq. (1) and using the variable separation approach, one can obtain the wave functions in three regions of the graphene waveguide

$$\boldsymbol{\psi}_{\mathrm{I}}(x,y,t) = \sum_{n=-\infty}^{\infty} \begin{bmatrix} e^{ik_{x,n}x} & e^{-ik_{x,n}x} \\ se^{i\phi_n}e^{ik_{x,n}x} & -se^{-i\phi_n}e^{-ik_{x,n}x} \end{bmatrix} \begin{bmatrix} \delta_{n,0} \\ r_n \end{bmatrix} \exp(ik_y y)\exp\left(-i\frac{E+n\hbar\omega}{\hbar}t\right), \tag{4a}$$

$$\boldsymbol{\psi}_{\mathrm{II}}(x,y,t) = \sum_{m,n=-\infty}^{\infty} J_n\left(\frac{U_1}{\hbar\omega}\right) \begin{bmatrix} e^{iq_{x,m}x} & e^{-iq_{x,m}x} \\ s'e^{i\varphi_m}e^{iq_{x,m}x} & -s'e^{-i\varphi_m}e^{-iq_{x,m}x} \end{bmatrix} \begin{bmatrix} a_m \\ b_m \end{bmatrix} \exp(ik_y y)\exp\left(-i\frac{E+m\hbar\omega+n\hbar\omega}{\hbar}t\right), \tag{4b}$$

$$\boldsymbol{\psi}_{\mathrm{III}}(x,y,t) = \sum_{n=-\infty}^{\infty} \begin{bmatrix} e^{ik_{x,n}x} & e^{-ik_{x,n}x} \\ se^{i\phi_n}e^{ik_{x,n}x} & -se^{-i\phi_n}e^{-ik_{x,n}x} \end{bmatrix} \begin{bmatrix} t_n \\ 0 \end{bmatrix} \exp(ik_y y)\exp\left(-i\frac{E+n\hbar\omega}{\hbar}t\right), \tag{4c}$$

where $s = \mathrm{sgn}(E + n\hbar\omega)$, $k_{x,n} = [(E+n\hbar\omega)^2/\hbar^2 v_f^2 - k_y^2]^{1/2}$, $\phi_n = \arctan(k_y/k_{x,n})$, $s' = \mathrm{sgn}(E + U_0 + m\hbar\omega)$, $J_n(U_1/\hbar\omega)$ is the Bessel function of the first kind and $q_{x,m} = (1-\lambda_x\varepsilon)^{-1}[(E+U_0+m\hbar\omega)^2/\hbar^2 v_f^2 - (1-\lambda_y\varepsilon)^2(k_y - q_{Dy})^2]^{1/2}$.

Strain-tunable guided mode. Since the bound state is caused by total internal reflection (TIR) at the p–n interface, the guiding of electrons is localized in the middle well region and the evanescent states exist in the left and right barrier regions. This means that the wavevector $q_{x,m}$ in the well region should be real and the wavevector $k_{x,n}$ in the left and right barrier regions is imaginary, which leads to

$$|E + U_0 + m\hbar\omega| > \hbar v_f|1-\lambda_y\varepsilon||k_y - q_{Dy}|, \tag{5a}$$
$$|E + n\hbar\omega| < \hbar v_f|k_y|. \tag{5b}$$

Therefore, $|E + U_0 + m\hbar\omega| = \hbar v_f|1-\lambda_y\varepsilon||k_y - q_{Dy}|$ and $|E + n\hbar\omega| = \hbar v_f|k_y|$ denote the boundaries between continuous states and bound states and are plotted in Fig. 1 (red dashed lines). Owing the unequal group velocities between the strained graphene region and the free graphene region,[21] one can rewrite the wave function in this form of $\boldsymbol{\psi}(x) = [1-\lambda\varepsilon(x)]^{-1/2}\boldsymbol{\Phi}(x)$, where $\varepsilon(x) = \varepsilon\,\Theta(w/2 - |x|)$ with $\Theta(x)$ as the Heaviside step function is the position-dependent strain modulus and $\boldsymbol{\Phi}(x)$ is a continuous function at the barrier's boundaries, to ensure the requirement of continuity equation. Therefore, according to the continuity of $\boldsymbol{\Phi}(x)$, we can obtain the energy spectrum of the bound states, which satisfies the following transcendental equation:

$$\begin{aligned}&[(E+n\hbar\omega)(E+U_0+m\hbar\omega) - (\hbar v_f)^2 k_y(1-\lambda_y\varepsilon)(k_y - q_{Dy})]\sin q_x w \\ &\quad + [(\hbar v_f k_y)^2 - (E+n\hbar\omega)^2]^{1/2}[(E+U_0+m\hbar\omega)^2 - (\hbar v_f)^2(1-\lambda_y\varepsilon)^2(k_y-q_{Dy})^2]^{1/2}\cos q_x w = 0.\end{aligned} \tag{6}$$

Because strain induces anisotropic Fermi velocity and a distribution of Fermi velocity has a strong influence on guided modes,[24] different direction strains will lead to different effects on the guided modes. We pay attention to double typical direction strains including the zigzag ($\theta = 0°$) and armchair ($\theta = 90°$) directions. The energy spectrum $E(k_y)$ is plotted in Fig. 1 (blue solid lines). In this calculation, some parameters are used: $\varepsilon = 2$, 8, and 14%, for zigzag direction strain, $\varepsilon = 0.5$, 1, and 1.5% for armchair direction strain, and in two cases, $U_0 = 40$ meV, $U_1 = 0$ meV, and $w = 150$ nm. Note that guided modes for a specific transverse wave vector can be determined by the intersections between energy spectrum and fixed k_y, such as $k_y = 0.05$ in Figs. 1(a)–1(c) and $k_y = 0.08$ in Figs. 1(d)–1(f). It is clearly seen that the guided modes and energy spectrum are changed by the strain. Indeed, strain effects of

Table I. Energy positions (meV) of guided mode and tunneling peak.

	Zigzag direction strain			Armchair direction strain		
	$\varepsilon = 2\%$	$\varepsilon = 8\%$	$\varepsilon = 14\%$	$\varepsilon = 0.5\%$	$\varepsilon = 1\%$	$\varepsilon = 1.5\%$
E_g	26.09	28.71	28.94	45.09	48.15	51.77
E_p	40.09	42.71	42.94	59.10	62.15	65.77

the zigzag and armchair directions on guided modes exhibit remarkable differences. For the zigzag direction strain in Figs. 1(a)–1(c), the numbers of intersections are 5, 6, and 7 for $\varepsilon = 0.02$, 0.08, and 0.14, respectively, which indicate that the number of guided modes increases with the strengthened strain. However, the number of guided modes dramatically decreases under armchair direction strain, as shown in Figs. 1(d)–1(f), since the Dirac point moves toward the right. Not only the number but also the energy of the guided mode is changed by the varied strain. We only list the energy positions (E_g) of the highest-order guided mode in Table I. It is clear that the energy location of the highest-order mode increases with increased strain along the zigzag or armchair direction. In addition, we also find that other order guided modes have a similar variation trend with changed strain. Therefore, one can control the appearance of the higher-order guided modes by adjusting the strain. In other words, a tunable graphene waveguide can be realized by manipulating the strain. The strain not only can control the bound states but also has an obvious influence on the surface state,[14,25] which is referred to the state localized near the barrier edges. We also calculate the surface modes under the armchair direction strain with $\varepsilon = 1$ and 1.5% and plot the results in Figs. 1(e) and 1(f) (green solid line). It is clear that the surface modes are localized inside both Dirac cones, which also occurs in strain-induced graphene superlattices with resonant modes.[25)]

Photon-assisted tunneling. Propagating states through the quantum well require that both the wavevector $q_{x,m}$ in the well region and the wavevector $k_{x,n}$ in the left and right barrier regions should be real, which leads to

$$|E + U_0 + m\hbar\omega| > \hbar v_f |1 - \lambda_y \varepsilon||k_y - q_{Dy}|, \tag{7a}$$

$$|E + n\hbar\omega| > \hbar v_f |k_y|. \tag{7b}$$

Matching the wave functions $\mathbf{\Phi}(x)$ at boundaries, one can obtain an infinite set of coupled equations consisting of unknown coefficients r_n, a_m, b_m, and t_n in Eqs. (4a)–(4c). However, the infinite series can be truncated to $2N + 1$ equations,[26] where N is a positive integer greater than $U_1/\hbar\omega$. Afterward, the transmission probability can be obtained by $T = \sum_{n=-N}^{N} |t_n|^2$. Figure 2 shows the transmission probability as a function of incident energy. In this calculation, $U_1 = 1$ meV, $\hbar\omega = 14$ meV, $N = 3$, and other parameters are identical to those in Fig. 1. One can clearly observe that some sharply asymmetric tunneling peaks occur and their energy positions vary with the changed strain. To compare with the energy of guided modes, we also show energy positions (E_p) of tunneling peaks in Table I. Remarkably, $E_p = E_g + \hbar\omega$; this means that the underlying mechanism is the typical photon-assisted tunneling process. In other words, incident electrons emit photons firstly, then drop to the highest-order bound state of the quantum well and finally tunnel through the well. By contrast, if the energy of incident electrons is less than that of the bound state, the incident electrons should absorb photons and then jump to the bound state. Similarly, incident electrons can also be transferred to other order bound states by changing the frequency (ω). More importantly, owing to the one-to-one correspondence between the energy position of the asymmetric tunneling peak and that of the guided mode, the photon-assisted tunneling can be utilized to probe the guided modes of the graphene waveguide.

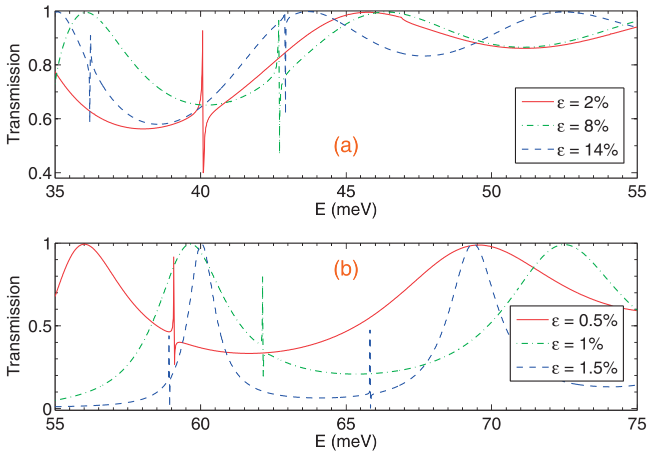

Fig. 2. Transmission probability as a function of incident energy for $U_0 = 40$ meV, $U_1 = 1$ meV, $\hbar\omega = 14$ meV, and $w = 150$ nm; (a) under zigzag direction strain at $k_y = 0.05$; (b) under armchair direction strain at $k_y = 0.08$.

One may wonder if the examination of the guided modes is available due to the transmission measurement and the smoothness of strain and potential profiles. For the transmission measurement, a previous experiment has shown that the transmission through the graphene waveguide can be measured.[12] It is shown that the transmission (T) is obtained by a 'focusing' geometry, with current I and applied voltage V, which lead to $T = h/2e^2R$ with the resistance R measured by using I–V curves.[12] To explore the influence of the smoothness of the interface on the detection of guided modes, we adopt a typical potential profile[27] and strain profile[21]

$$U_{0,1}(x) = 0.5U_{0,1}\left[\mathrm{erf}\left[\frac{2w(x + w/2)}{d - 2}\right] + \mathrm{erf}\left[\frac{2w(w/2 - x)}{d - 2}\right]\right], \tag{8a}$$

$$\varepsilon(x) = \frac{\varepsilon}{\tanh(w/4a)}\left(\frac{1}{1 + \exp[-(x + w/2)/a]} - \frac{1}{1 + \exp[-(x - w/2)/a]}\right), \tag{8b}$$

where $\mathrm{erf}(x)$ is the error function with smoothing parameter d and a. The numerical results are plotted in Fig. 3. It is clearly observed that the smoothness of the interface has an obvious influence on the guided mode. Under zigzag direction strain, the guided mode is dependent on the potential profile, but independent of the strain profile, as shown in

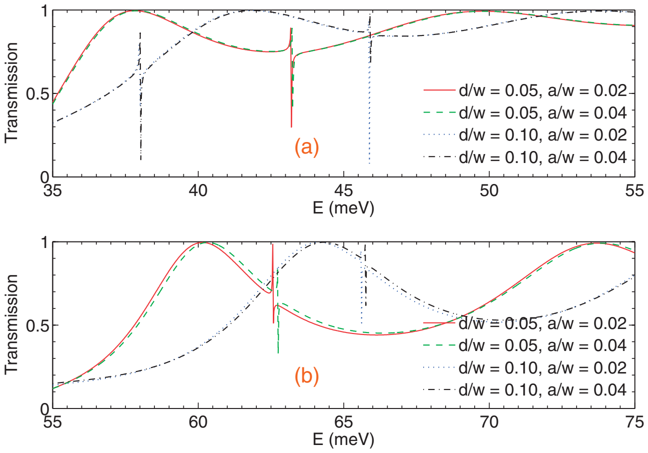

Fig. 3. Transmission probability as a function of incident energy for real potential profile $U_{0,1}(x)$ and strain profile $\varepsilon(x)$ in Eq. (8), with $U_0 = 40\,\text{meV}$, $U_1 = 1\,\text{meV}$, $\hbar\omega = 14\,\text{meV}$, and $w = 150\,\text{nm}$; (a) under zigzag direction strain of $\varepsilon = 2\%$ at $k_y = 0.05$; (b) under armchair direction strain of $\varepsilon = 0.5\%$ at $k_y = 0.08$.

Fig. 3(a). Under armchair direction strain, the guided mode in Fig. 3(b) is dependent on not only the potential profile but also the strain profile. However, the asymmetric tunneling peak remains in all cases. Therefore, the smoothness of the strain and potential profiles will not restrict the application of the photon-assisted tunneling. In other words, it is available to probe guided modes in the graphene waveguide based on the photon-assisted tunneling.

In summary, we have explored the strain effect on guided mode in a graphene waveguide. Numerical results indicate that the number of guided modes increases under zigzag direction strain. However, the number decreases under armchair direction strain due to the displacement of Dirac points. We also have investigated the electron transmission through a strained graphene waveguide with an oscillating potential, as a function of incident energy. It is found that the transmission spectrum displays a sharply asymmetric tunneling peak and the energy difference between the tunneling peak and guided mode is equal to the photons induced by the oscillating potential. Therefore, from the tunneling peak, one can obtain information on the guided mode in a graphene waveguide and further examine the strain effect on the guided modes.

Acknowledgment We are grateful for the support from NSFC (Nos. 10902128, 10732100, and 11072271).

1) V. V. Cheianov, V. Fal'ko, and B. L. Altshuler: Science **315** (2007) 1252.
2) J. Cserti, A. Pályi, and C. Péterfalvi: Phys. Rev. Lett. **99** (2007) 246801.
3) C. W. J. Beenakker, R. A. Sepkhanov, A. R. Akhmerov, and J. Tworzydło: Phys. Rev. Lett. **102** (2009) 146804.
4) Z. Wu, F. Zhai, F. M. Peeters, H. Q. Xu, and K. Chang: Phys. Rev. Lett. **106** (2011) 176802.
5) C. E. P. Villegas and M. R. S. Tavares: Appl. Phys. Lett. **101** (2012) 163104.
6) A. V. Rozhkov, G. Giavaras, Y. P. Bliokh, V. Freilikher, and F. Nori: Phys. Rep. **503** (2011) 77.
7) Y. P. Bliokh, V. Freilikher, and F. Nori: Phys. Rev. B **81** (2010) 075410.
8) H. Li, L. Wang, Z. Lan, and Y. Zheng: Phys. Rev. B **79** (2009) 155429.
9) J. Milton Pereira, Jr., V. Mlinar, F. M. Peeters, and P. Vasilopoulos: Phys. Rev. B **74** (2006) 045424.
10) F. M. Zhang, Y. He, and X. Chen: Appl. Phys. Lett. **94** (2009) 212105.
11) Z. Wu: Appl. Phys. Lett. **98** (2011) 082117.
12) J. R. Williams, T. Low, M. S. Lundstrom, and C. M. Marcus: Nat. Nanotechnol. **6** (2011) 222.
13) B. Özyilmaz, P. Jarillo-Herrero, D. Efetov, D. A. Abanin, L. S. Levitov, and P. Kim: Phys. Rev. Lett. **99** (2007) 166804.
14) V. M. Pereira and A. H. Castro Neto: Phys. Rev. Lett. **103** (2009) 046801.
15) V. M. Pereira, A. H. Castro Neto, and N. M. R. Peres: Phys. Rev. B **80** (2009) 045401.
16) C. Lee, X. Wei, J. W. Kysar, and J. Hone: Science **321** (2008) 385.
17) K. S. Kim, Y. Zhao, H. Jang, S. Y. Lee, J. M. Kim, K. S. Kim, J. H. Ahn, P. Kim, J. Choi, and B. H. Hong: Nature **457** (2009) 706.
18) Z. H. Ni, T. Yu, Y. H. Lu, Y. Y. Wang, Y. P. Feng, and Z. X. Shen: ACS Nano **2** (2008) 2301.
19) M. Y. Huang, H. Yan, T. F. Heinz, and J. Hone: Nano Lett. **10** (2010) 4074.
20) S. M. Choi, S. H. Jhi, and Y. W. Son: Phys. Rev. B **81** (2010) 081407(R).
21) F. M. D. Pellegrino, G. G. N. Angilella, and R. Pucci: Phys. Rev. B **84** (2011) 195404.
22) F. Guinea, M. I. Katsnelson, and A. K. Geim: Nat. Phys. **6** (2010) 30.
23) M. Wagner: Phys. Rev. A **51** (1995) 798.
24) Y. Wang, Y. Liu, and B. Wang: Physica E **48** (2013) 191.
25) F. M. D. Pellegrino, G. G. N. Angilella, and R. Pucci: Phys. Rev. B **85** (2012) 195409.
26) The Bessel function $J_{n>N}(U_1/\hbar\omega)$ of the first kind is very small and can be negligible.
27) F. Zhai, Y. Ma, and K. Chang: New J. Phys. **13** (2011) 083029.